Chapter IV

Adsorption Studies using TPJB

The experimental results of divalent ions – treated ***Prosopis juliflora*** **Bark** (TPJB) systems from aqueous solutions and industrial effluents are dealt in this chapter.

4.1 Microscopic Studies

The lengths and breadths of measured granular particles were subjected to application of multiplication factor to the average values, from which the particle sizes were determined. Based on these values, microscopically calculated 0.18 mm, 0.21 mm, 0.30 mm, 0.42 mm and 0.71 mm sizes, corresponded to 85 BSS, 72 BSS, 52 BSS, 36 BSS and 22 BSS mesh sizes. The microscopic miniature of the chosen particle size (0.18mm) of TPJB is illustrated in figure 4.1.

4.2 BET and BJH Analyses

Evaluation of the particle/ mesopore size distribution of TPJB using BET and BJH methods (Figures 4.2 - 4.4). The adsorption performance is highly dependent on the internal pore structure. International Union of Pure and Applied Chemistry (IUPAC manual, 1982)[112] classified the pore size as; micropores (d<20Å), mesopores (20 Å < d< 500 Å) and macropores (d > 500 Å). Because of the larger sizes of the liquid molecules, as far as adsorbates are concerned, the adsorbents are expected to possess predominantly mesoporus nature[113]. The surface area and mean pore diameter calculated from BET/ BJH plots revealed 3.28 m^2/ g and 56.6 nm (Table 4.1) respectively. Thence, 0.18 mm size is considered as for further experiments.

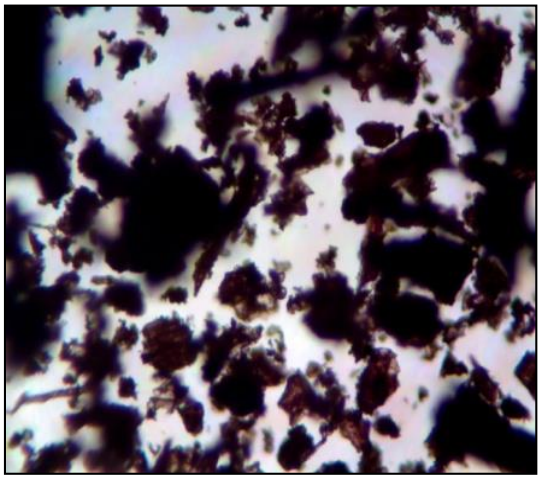

Figure 4.1 Microscopic View

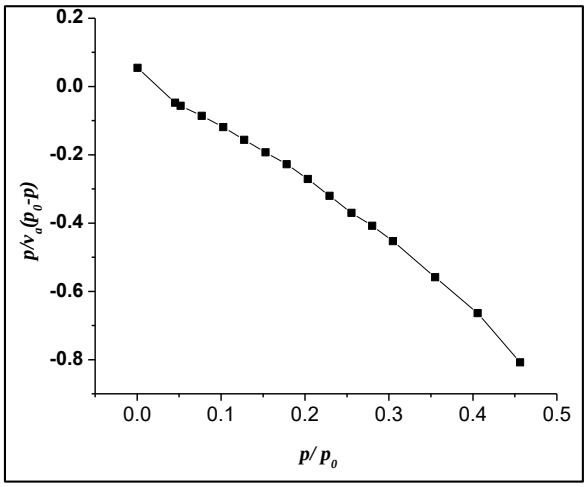

Figure 4.2 BET Plot

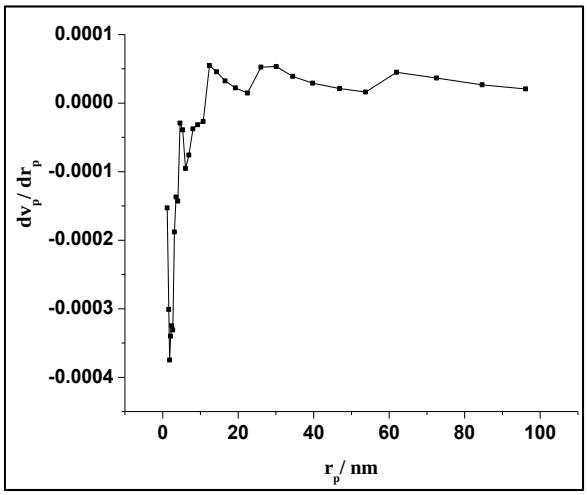

Figure 4.3 BJH Plot

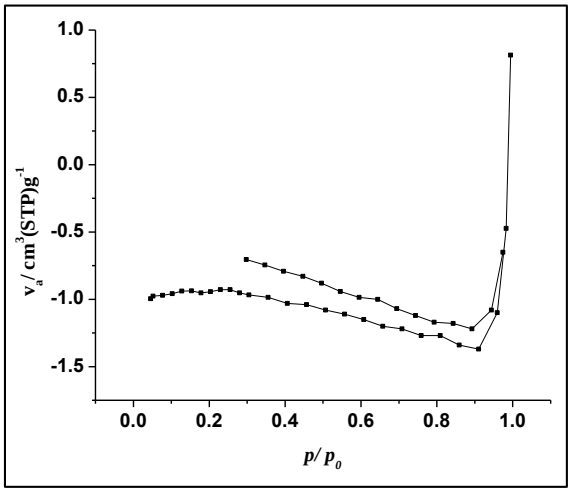

Figure 4.4 Adsorption/ Desorption Plot

4.3 TPJB - Characterization

The bulk density values (Table 4.1) is observed to be less than 1.2 g/L which implies the presence of fine porous particles supporting high metal sorption[114]. Moisture content is one of the factors that affect the activity of sorbent materials. The value being approximately 5%, i.e., 5.97 indicates favorable adsorption[115]. Specific gravity of TPJB (1.45) is found to be greater than that of water (1.00), revealing the lower surface tension favours the sorption process. pH_{zpc} is 5.51 < 7, indicate the negatively charged surface (arised due to the basic sites) which assists the affinity towards the cationic sorption of TPJB.

The lesser ash content value (3.93 %) supports the presence of high carbon content against inorganic matter[105]. From the results of C, H, N and S analyses, it is confirmed that the carbon percentage is higher than its counterparts. A comparative study regarding specific physicochemical parameters between TPJB and other reported materials had been made, which shows the better characteristic nature of the former (Table 4.1a)

Surface functional groups determined by Boehm titration method clearly indicate that the total acidic groups (carboxylic groups) are slightly greater than the total basic groups in the TPJB. In aqueous solutions, the acidic surface groups enriched with H^+ ions, undergo ionization where the protons leave TPJB surface resulting in the formation of negatively charged sites[116]. Thence, the electrostatic interaction is enhanced between the negatively charged surface of TPJB and the positively charged divalent ions, thereby reflecting in greater adsorption capacity[117].

Table 4.1 Physiochemical Characterization

Properties	TPJB
pH (1 % solution)	5.62
Conductivity	43.23
Moisture (%)	5.97
Bulk density (g/L)	0.63
Specific gravity	1.45
Porosity	56.55
Ash content (%)	3.93
Water soluble matter (%)	2.23
Acid soluble matter (%)	1.54
Ion exchange capacity (meq/g)	0.46
pH_{zpc}	5.51
Surface area (m^2/g)	3.281
Mean Pore diameter (nm)	56.6
Carbon (%)	44.95
Nitrogen (%)	0.67
Hydrogen (%)	4.69
Sulphur (%)	Nil
Surface Acidic Groups (mmol/g)	
Phenolic	0.72
Carboxylic	1.32
Lactonic	0.19

Table 4.1a Characteristics Comparison with Reported Literature

Adsorbents	Ash	Moisture	C	H	N	S
Holm oak[118]	5.3	9.5	48.0	5.9	0.5	_
Cashew nut shell[119]	5.7	9.8	45.2	4.2	0.2	_
Tea waste[120]	4.8	6.4	47.0	8.2	0.4	0.5
Pyrenean oak[118]	5.4	11.1	48.5	5.9	0.5	0.01
Sugarcane leaves[121]	7.7	_	39.7	5.5	_	0.2
Moringa oleifera bark[122]	11.1	7.5	44.8	5.9	0.8	0.9
Sunflower waste[123]	3.8	6.8	44.0	2.8	8.5	_
Wheat straw[124]	7.7	_	46.7	6.3	0.4	0.1

4.4 SEM and EDAX Analyses

The appearance of highly porous morphology and coarse surface texture with pores of different shapes (Figure 4.6) for unloaded TPJB recorded a better pore pattern than the corresponding image of raw material (Figure 4.5). TPJB had registered a remarkable physical change over the adsorption period, as compared to that of the unloaded materials, which is indicated by the integrated and cluster arrangements[125] for Pb(II), Cd(II) and Ni(II) ions laden sorbent surface (Figures 4.7- 4.9).

Presence of Pb(II), Cd(II) and Ni(II) ion peaks at 2- 8 keV substantiate the adsorption on TPJB (Figures 4.11 - 4.13) against their absence in the unloaded spectra (Figure 4.10).

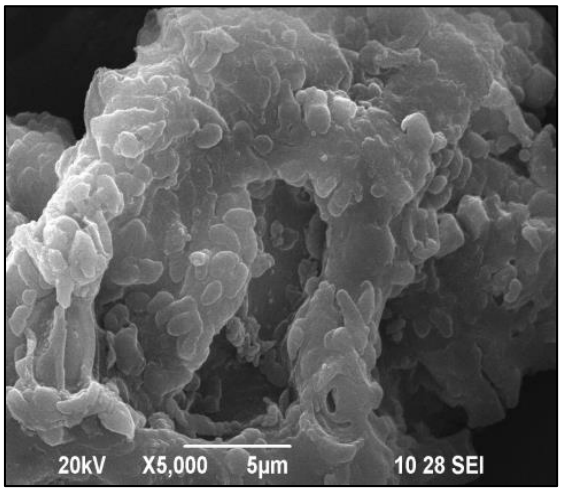

Figure 4.5 SEM: PJB

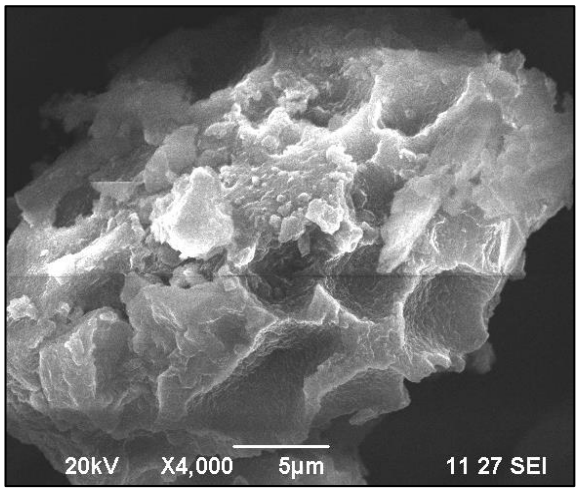

Figure 4.6 SEM: TPJB

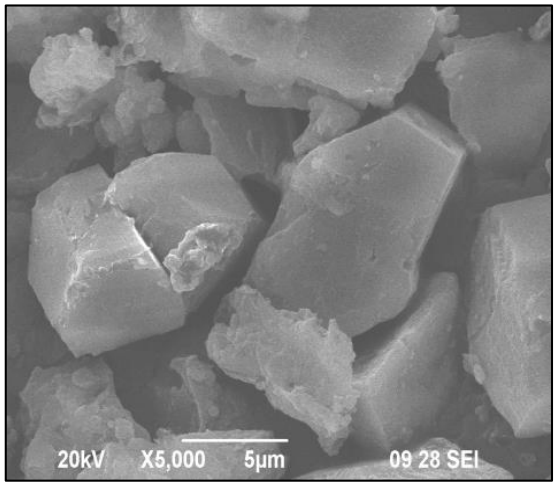

Figure 4.7 SEM: Pb(II) -TPJB

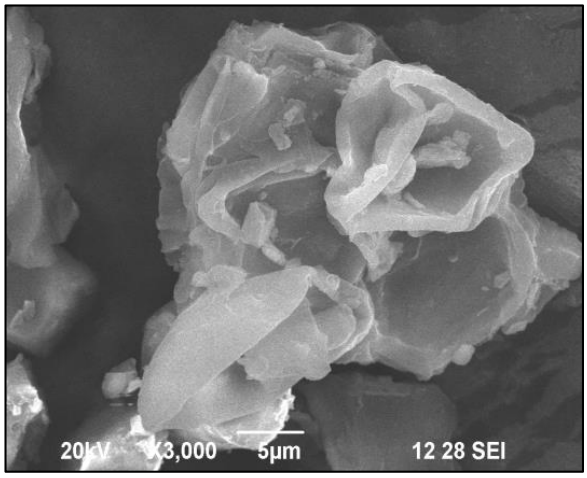

Figure 4.8 SEM: Cd(II) - TPJB

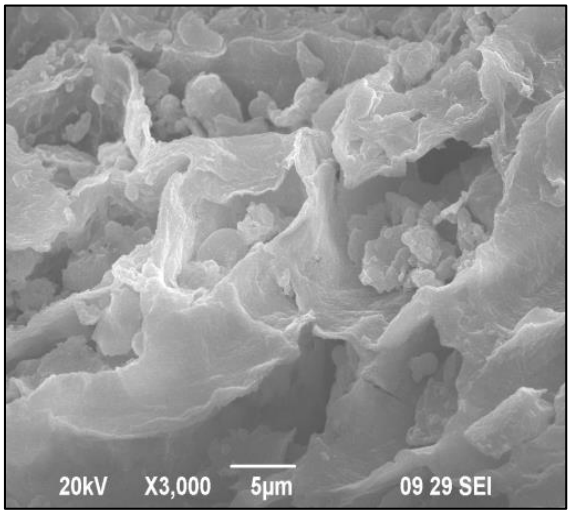

Figure 4.9 SEM: Ni(II) - TPJB

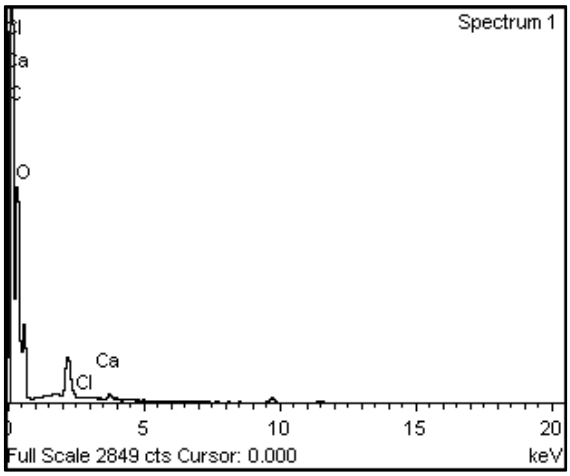

Figure 4.10 EDAX: TPJB

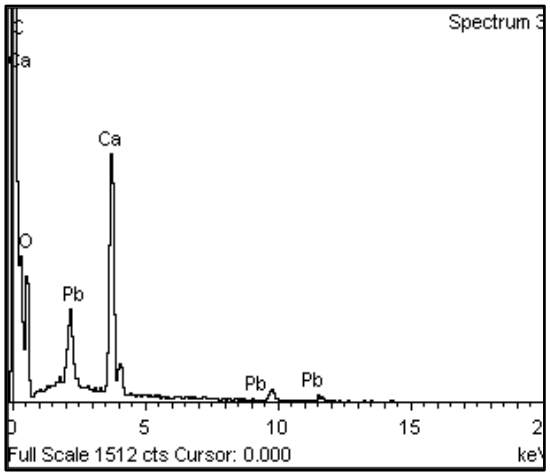

Figure 4.11 EDAX: Pb(II) - TPJB

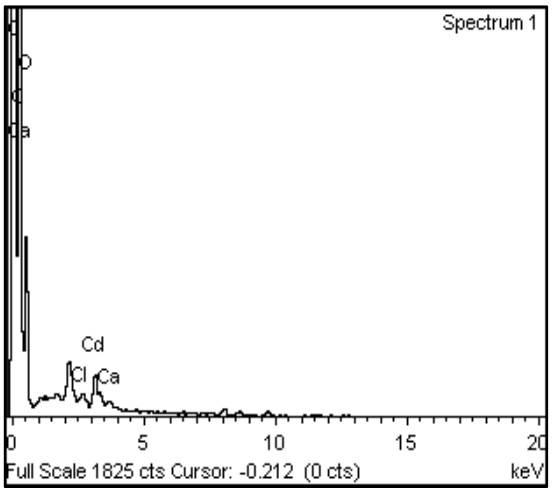

Figure 4.12 EDAX: Cd(II) - TPJB

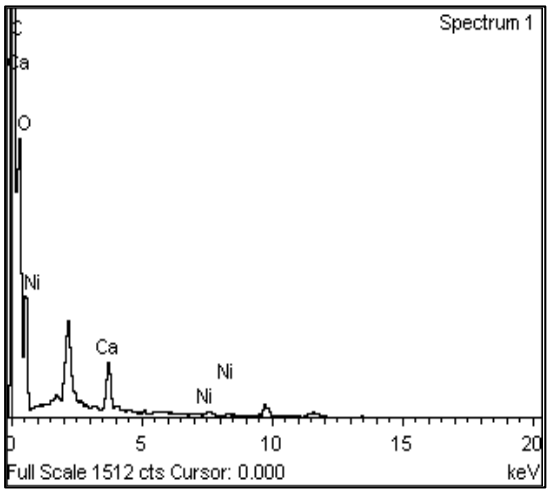

Figure 4.13 EDAX: Ni(II) - TPJB

4.5 FTIR Spectral Studies

The unloaded TPJB [Figure 4.14(a)] shows prominent peaks corresponding to O-H (3716.95 cm^{-1}), H-C-H (2306.96 cm^{-1}), C=O (1746.62 cm^{-1}), C-H (1443.78 cm^{-1}) and C-O (1042 cm^{-1}, 1025 cm^{-1}) functional groups, occurring at respective wavelengths. FTIR spectra of Pb(II) loaded TPJB is shown in figure 4.14 (b) wherein, the shifts in peak values are observed as: O-H (3773.89 cm^{-1}), H-C-H (2378.83 cm^{-1}), C=O (1738.90 cm^{-1}), C-H (1440.89 cm^{-1}) and C-O (1032.93 cm^{-1}) favouring Pb(II) adsorption. Disappearance of O-H / C=O peaks and shifts in H-C-H (2305.03 cm^{-1}) and C-H (1518.04 cm^{-1}) bands in Cd(II) loaded spectra [Figure 4.14 (c)], suggest deprotonation, followed by the probable formation of metal oxygen bond during Cd(II) sorption. A shift in the position of few functional groups viz., O-H (3776.17 cm^{-1}), C=O (1740.83 cm^{-1}), C-H (1367.59 cm^{-1}) and

C-O (1032.93 cm^{-1}) is noticed in Ni(II) laden TPJB [Figure 4.14(d)] support the respective changes, which can be attributed to electrostatic interactions[126] between the functional groups of TPJB and specific sorbate species.

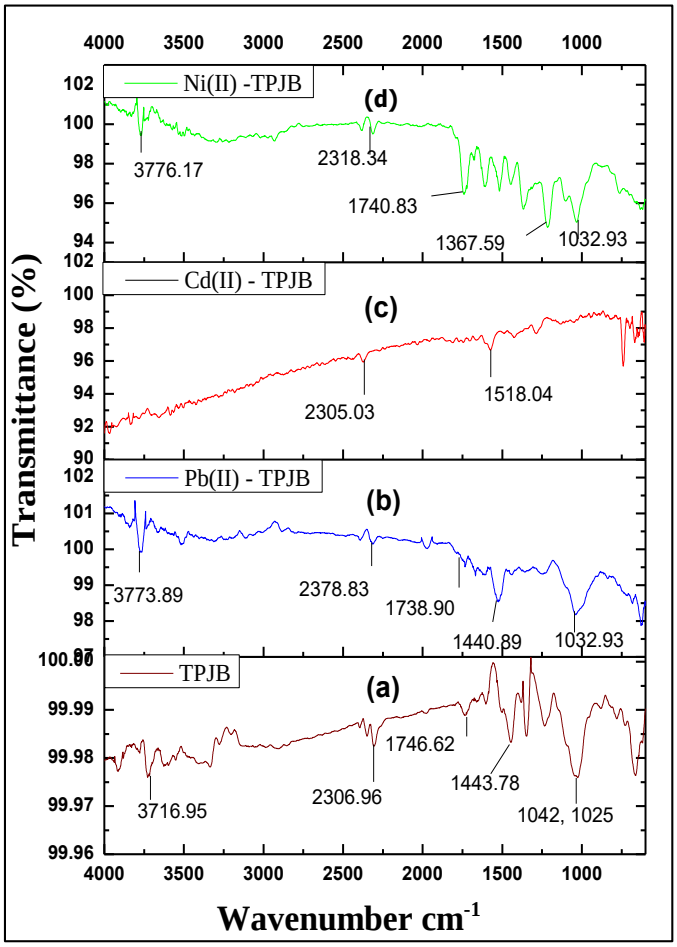

Figure 4.14 FTIR Spectra

4.6 Batch Equilibration Experiments

4.6.1 Effect of Particle Size

An increase in the sorption of Pb(II), Cd(II) and Ni(II) ions with decreasing particle size is obvious from figure 4.15, which shall be due to the surface phenomenon; the smaller particle size offers larger surface area for enhanced removal of metal ions[127]. Thus, 0.18mm being the smaller chosen particle size exhibited greater 'q_e' values (Table 4.2) of the three systems, 'q_e' values of Pb(II) sorption is higher being validated by the gradient decline of the systematic curves. The lower hydrated ionic radii of Pb(II) [4.01 Å] <

Cd(II)/ Ni(II) reveals its best sorptive nature than the counter ions[128]. The context of smaller particle size leading to greater sorption is found in other reports using rice husk[129] and citrus peels[99].

Table 4.2 Effect of Particle Size

Metal Ions	Amount Adsorbed (mg/g)				
	0.18 mm	**0.24 mm**	**0.30 mm**	**0.42 mm**	**0.71 mm**
Pb(II)	**14.18**	13.69	12.53	11.71	10.72
Cd(II)	**13.54**	12.71	12.38	11.55	11.06
Ni(II)	**12.32**	11.18	9.89	9.56	8.59

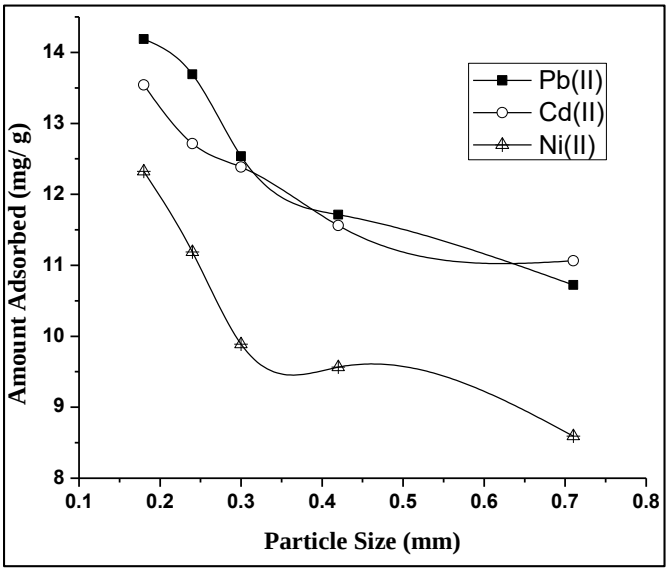

Figure 4.15 Effect of Particle Size

4.6.2 Effect of Initial Concentration and Agitation Time

Amidst the varying concentrations studied, an initial concentration of 100 mg/ L recorded maximum sorption as evident from the figures 4.16 – 4.18. The decline in sorption rate may be due to the saturation of surface sites[130]. Also, TPJB is observed to adsorb Pb(II) ions in preference to Cd(II) and Ni(II) ions whose 'q_e' values are listed in table 4.3.

The rapid initial uptake of divalent ions is probably due to the abundant availability of active sites on TPJB surface, where an initial contact time of 30 minutes had furnished maximum sorption, after which the system reaches equilibrium[131]. Thus, the optimized conditions for forthcoming experiments are fixed as 100 mg/L initial concentration and 30 minutes preset time intervals.

Table 4.3 Effect of Initial Concentration and Agitation Time

Metal Ions	Time (min)	Amount Adsorbed (mg/g)				
		50 mg/L	100 mg/L	150 mg/L	200 mg/L	250 mg/L
Pb(II)	10	9.24	13.16	11.68	11.90	12.71
	20	9.60	13.56	11.53	12.08	13.13
	30	9.91	**14.22**	11.82	12.65	13.86
	40	9.81	13.89	11.44	12.27	13.68
	50	9.48	13.40	11.56	12.46	13.17
	60	9.12	12.90	11.32	12.28	12.71
Cd(II)	10	7.11	13.33	10.76	11.77	12.05
	20	7.58	13.55	11.05	12.15	12.29
	30	8.06	**13.68**	11.64	12.72	12.98
	40	7.70	13.17	11.35	12.15	12.82
	50	7.82	13.44	11.49	11.39	12.71
	60	7.94	13.17	10.61	11.20	12.53
Ni(II)	10	6.67	11.53	8.82	10.47	10.83
	20	7.02	12.19	9.56	10.80	11.27
	30	7.38	**12.52**	10.15	10.97	11.49
	40	7.26	12.36	9.85	10.31	11.05
	50	7.14	11.70	9.98	9.81	10.61
	60	6.90	11.53	9.71	9.47	9.94

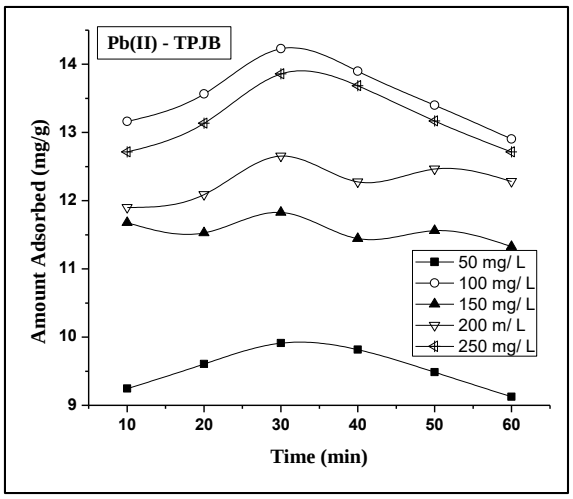

Figure 4.16 Effect of Initial Concentration and Agitation Time- Pb(II)

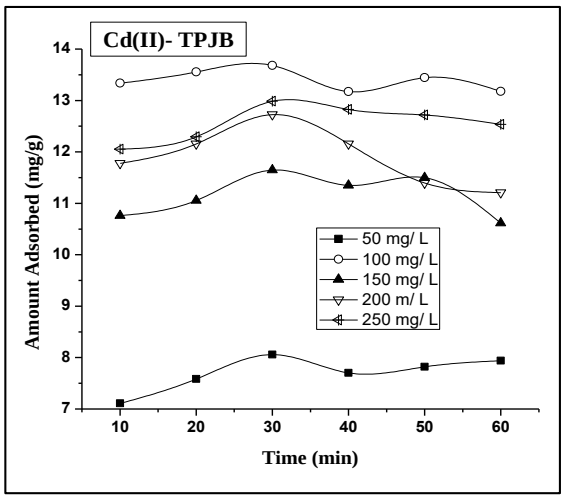

Figure 4.17 Effect of Initial Concentration and Agitation Time- Cd(II)

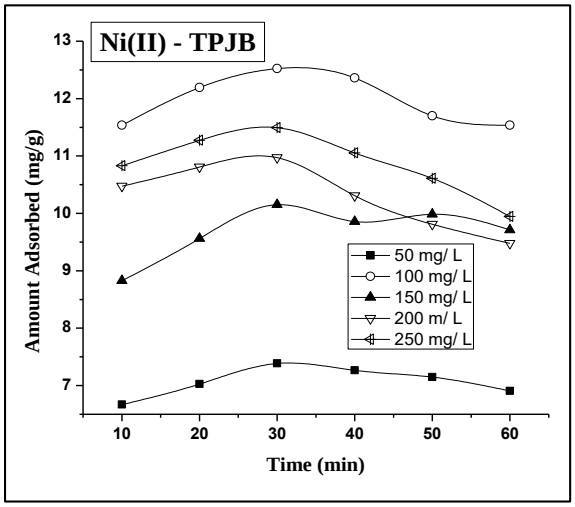

Figure 4.18 Effect of Initial Concentration and Agitation Time- Ni(II)

4.6.3 Effect of Dosage

Figure 4.19 shows the decline of curves with increase in sorbent dose (100 – 500 mg) for an initial concentration of 100 mg/L. A maximum adsorption had occurred at 300 mg, fixed as the optimized dose invariably for all the systems.

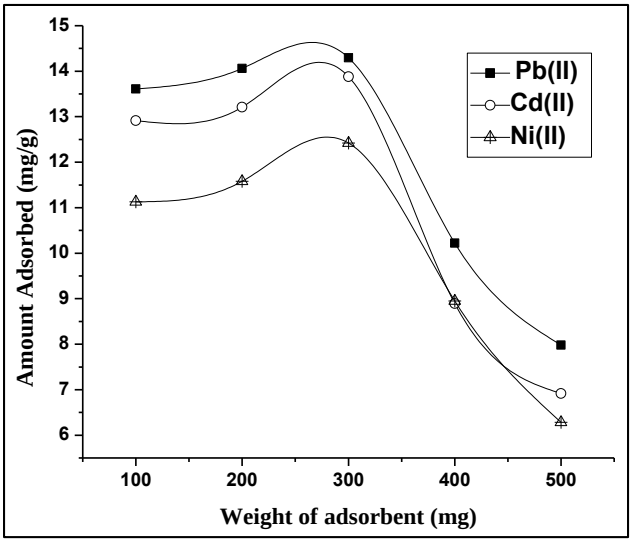

Figure 4.19 Effect of Adsorbent Dose

4.6.4 Effect of pH

It is apparent from table 4.4, that the amounts of Pb(II), Cd(II) and Ni(II) adsorbed are maximum at pH 5, 7 and 5. At low and higher pH values, the system register a decline which shall be recognized as the higher electronegative characteristics[132, 133, 134] (polar groups like -COOH, -OH etc) of the TPJB.

Table 4.4 Effect of pH

pH	Amount Adsorbed (mg/ g)		
	Pb(II)	**Cd(II)**	**Ni(II)**
3	10.72	9.90	9.05
5	**14.29**	10.03	**12.52**
7	12.63	**13.87**	8.02
9	10.37	7.37	6.97
11	9.08	6.03	6.07

4.6.5 Effect of Cations/ Anions/ Co-ions

Presence of few inorganic ions such as potassium, magnesium, sulphate, chloride, apart from the occurrence of co-ions like chromium, zinc in the industrial discharges are imperative to study their influence in the removal of Pb(II), Cd(II) and Ni(II) by TPJB. The impact of these

ions are shown in table 4.5, from which it is obvious that, marked inhibition is exhibited by K^+ rather than Mg^{2+} for all the three metal systems. The reason could be explained in terms of ionic radii[135] (1.38Å - K^+ ions and 0.72 Å - Mg^{2+} ions), where smaller radius of Mg^{2+} minimizes its swelling pressure within the aqueous matrix[136], thereby promotes metal sorption on TPJB surface. Formation of highly soluble chloro complexes of metal ions, may support the fact of less availability of divalent ions, thereby inclined inhibition of chloride ions is obvious in compared with SO_4^{2-} ions. As far as, co-ionic influence is concerned, the metal binding property of TPJB is little affected, thereby favouring the sorption capacity, more in case of Pb(II), Cd(II), Ni(II) than Zn(II) and Cr(VI) ions.

Table 4.5 Effect of Cations, Anions and Co-ions

Metal Ions	Percentage Removal (%)						
	Absence of Ions	Cations		Anions		Co-ions	
		K^+	Mg^{2+}	Cl^-	SO_4^{2-}	Zn^{2+}	Cr^{6+}
Pb(II)	86.04	78.63	80.81	76.07	79.52	84.79	82.58
Cd(II)	82.42	76.47	78.56	76.13	77.26	80.84	79.05
Ni(II)	76.18	72.48	73.74	69.55	71.68	71.53	70.54

4.6.6 Effect of Temperature

Table 4.6 lists the data pertaining to varied temperature environments; a steady increase in the percentage removal is evident with temperature, which reflects the mobility of surface active sites and reduction in the boundary layer thickness, in turn restricting the mass transfer resistance of chosen metal ions [137, 108].

Table 4.6 Effect of Temperature

Temperature (K)	Percentage Removal (%)		
	Pb(II)	Cd(II)	Ni(II)
293	77.56	72.85	67.34
303	86.04	82.42	76.18
313	88.63	84.17	77.09
323	89.32	85.56	78.21
333	91.56	87.04	78.87

4.6.7 Desorption/ Regeneration Studies

Desorption of loaded metal ions from the surface of TPJB with HCl as eluent was observed to vary linearly with the concentrations of the acid (0.01 to 0.05 M): as obvious from table 4.7.

A maximum of 80.20, 79.05 and 72.64 percentage desorption for Pb(II), Cd(II), Ni(II) respectively is evident and thence 0.05 M HCl was fixed for regeneration cycles. The three regeneration cycles on chosen divalent ions are shown as bar chart (Figure 4.20) and the corresponding retention capacity was found to be 78, 75 and 70.5%, beyond which a decline was envisaged.

Table 4.7 Desorption

HCl Concentration (M)	Percentage Removal (%)		
	Pb(II)	Cd(II)	Ni(II)
0.01	71.34	66.64	67.03
0.02	73.72	69.06	70.24
0.03	75.52	72.85	71.89
0.04	78.89	75.23	71.28
0.05	**80.20**	**78.05**	**72.64**

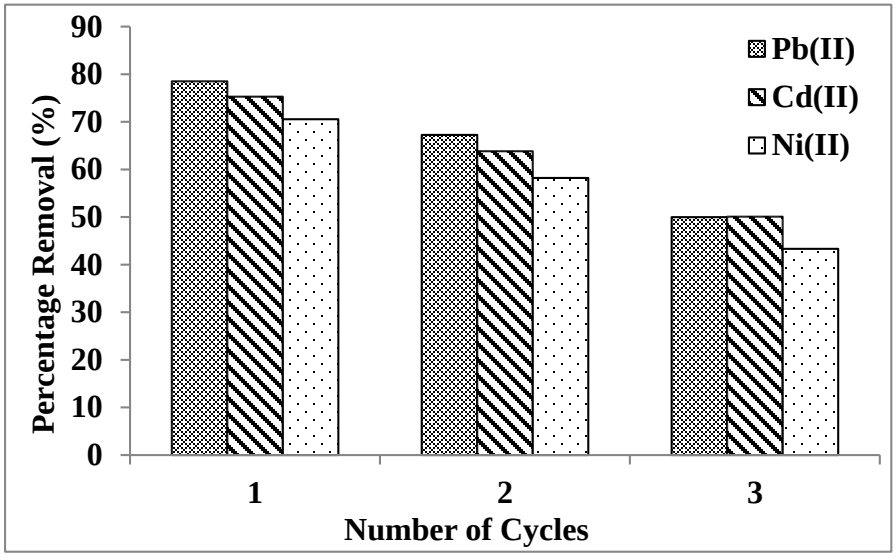

Figure 4.20 Regeneration - TPJB

4.7 Adsorption Isotherms

Langmuir, Freundlich, Tempkin and Dubinin- Radushkevich isothermal equations applied to the experimental data and their constant parameters calculated from the linearized equations are listed in tables 4.8 and 4.9 respectively.

Table 4.8 Equilibrium Concentrations

Conc. of Metal Ions (mg/L)	Langmiur		Freundlich		Tempkin		DKR	
	C_e	C_e/q_e	log C_e	log q_e	ln C_e	q_e	ε^2 X10^{-5}	ln q_e
Pb(II)								
50	8.38	0.84	0.92	0.99	2.12	9.91	0.13	2.29
100	13.88	0.97	1.14	1.01	2.63	11.22	0.02	2.71
150	31.44	2.65	1.49	1.07	3.44	11.82	0.06	2.47
200	62.33	4.92	1.79	1.10	4.13	12.65	0.01	2.53
250	88.46	6.38	1.94	1.14	4.48	13.86	0.008	2.62
Cd(II)								
50	15.17	1.88	1.18	1.03	2.71	11.06	0.25	2.08
100	16.70	1.22	1.22	1.03	2.81	11.68	0.24	2.22
150	30.96	2.65	1.49	1.06	3.43	11.64	0.18	2.45
200	62.68	4.92	1.79	1.10	4.13	12.72	0.01	2.43
250	111.26	8.56	2.04	1.11	4.71	12.98	0.005	2.56
Ni(II)								
50	18.10	2.45	1.25	0.93	2.89	9.38	0.18	1.99
100	23.73	1.89	1.37	0.97	3.16	10.25	0.01	2.52
150	45.61	4.49	1.65	1.00	3.82	10.15	0.02	2.31
200	56.57	5.15	1.75	1.04	4.03	10.97	0.02	2.39
250	106.14	9.23	2.02	1.06	4.66	11.49	0.05	2.47

Table 4.9 Isothermal Constants

Isotherm Parameters	Pb(II)	Cd(II)	Ni(II)
Langmuir			
q_m (mg/g)	14.78	13.92	13.63
b (L/g)	0.15	0.32	0.19
R^2	0.9885	0.9899	0.9871
Freundlich			
K_F (mg/g)	7.28	8.31	5.68
n	7.18	10.23	6.45
R^2	0.9781	0.9665	0.9577
Tempkin			
A_T (L/g)	3.40	2.58	2.29
b_T	1.19	0.94	1.27
R^2	0.9091	0.8683	0.8034
DKR			
q_s (mg/g)	14.12	12.67	12.30
E (kJ/mol)	0.42	0.61	0.42
R^2	0.8181	0.8039	0.8620

4.7.1 Langmuir Isotherm Model

A linear plot (C_e/ q_e vs C_e) was obtained for the Langmuir model (Figure 4.21). The derived monolayer adsorption capacity (q_m) values from the plot is in good agreement with the q_e values of batch results for all the three ions. Higher b value is indicative of greater affinity[138] of TPJB towards the metal ions. The correlation coefficient R^2 values viz., 0.9885, 0.9899 and 0.9871 discloses the better linear fit. The calculated R_L values (Table 4.10) in the range (0.01 - 0.11) reveal favourable adsorption.

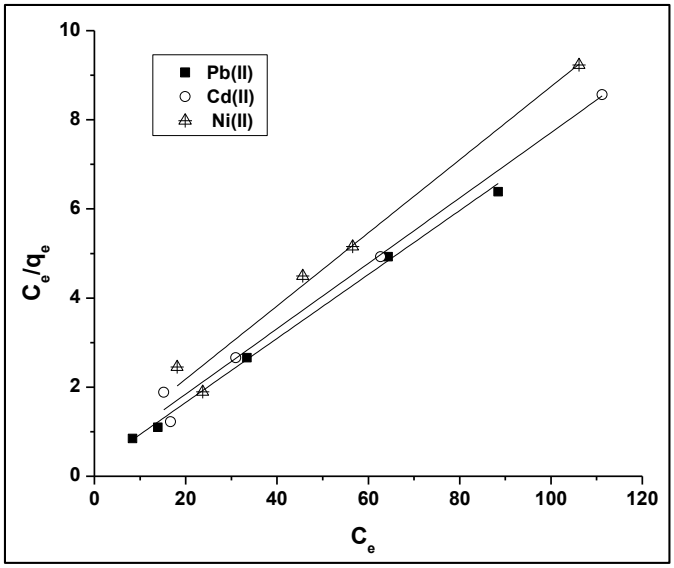

Figure 4.21 Langmuir Isotherm Model

Table 4.10 Equilibrium Parameter (R_L)

Conc. (mg/L)	Pb(II)	Cd(II)	Ni(II)
50	0.11	0.05	0.09
100	0.06	0.02	0.04
150	0.04	0.02	0.03
200	0.03	0.01	0.02
250	0.02	0.01	0.02

4.7.2 Freundlich Isotherm Model

The K_F and n values derived from the intercepts and slopes of the straight lines observed in the Freundlich plot (Figure 4.22) correspond to the adsorption capacity and sorption intensity of TPJB, where the 'n' values greater than unity and R^2 values, nearness to unity unfolds that the three systems obey Freundlich model [139, 140], however, the best fit is suited for Langmuir model, the reason being, q_m values are in good agreement with q_e values.

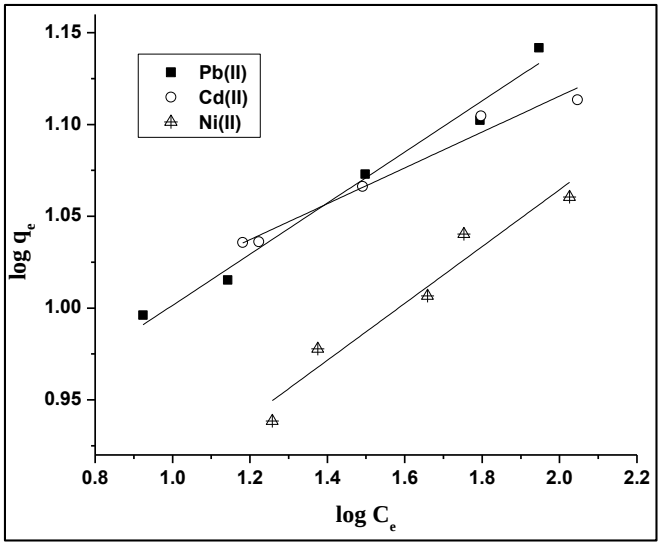

Figure 4.22 Freundlich Isotherm Model

4.7.3 Tempkin Isotherm Model

A plot of q_e vs ln C_e for Tempkin model suggests that the points are scattered, with no proper fit in the straight lines (Figure 4.23). As a result, lower A_T (binding constant) and b_T (heat of adsorption) values were derived from the plots, representing weak sorbate/ sorbent interactions which doesn't hold good for the studied systems. Correlation coefficient values observed as 0.9091, 0.8683, 0.8034 for Pb(II), Cd(II) and Ni(II), show that the systems do not favour Tempkin model.

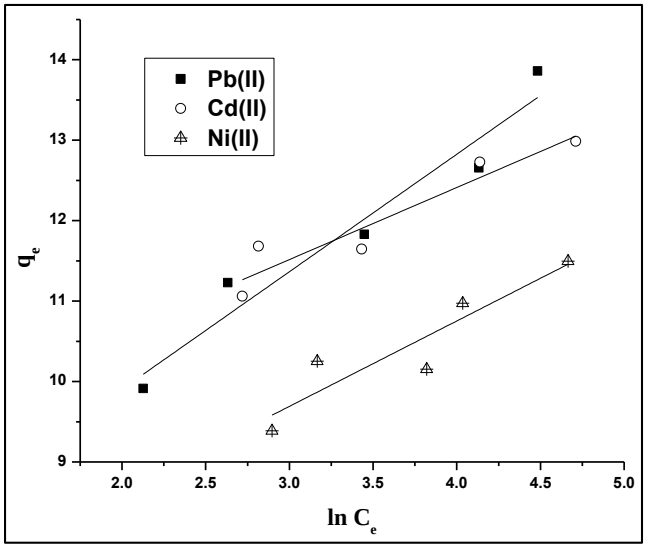

Figure 4.23 Tempkin Isotherm Model

4.7.4 Dubinin–Kaganer-Radushkevich Isotherm Model

The DKR plot (Figure 4.24) for the three systems reveal non-linear fit of the model supported by lower R^2 values. The calculated mean free energy values from the slope and intercept readings (Table 4.9) are observed to be 0.42, 0.61 and 0.42 KJ/ mol being lesser than 8 KJ/ mol imply the nature of sorption to be physisorption[108].

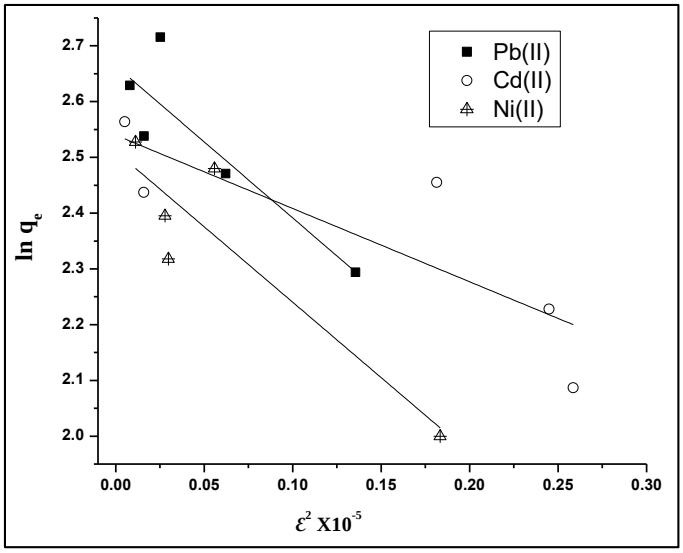

Figure 4.24 Dubinin-Kaganer-Radushkevich Isotherm Model

4.8 Adsorption Kinetics

Pseudo-first-order and pseudo-second-order kinetics suggested by Lagergren model[141] and Ho/ Mc Kay[142], along with Elovich and Intraparticle diffusion models are discussed here.

4.8.1 Pseudo-First-Order Model

Batch experimental results [optimum adsorption capacity (q_{exp}) and the amounts adsorbed at respective time frames (q_t)] were verified using pseudo-first order equation (Table 4.11), from which the graph of log (q_e–q_t) vs t (Figure 4.25) is plotted.

The first- order rate constant k_1 and equilibrium adsorption capacity q_{cal} derived from the slopes and intercepts, along with R^2, SSE values are shown in table 4.12. Correlation coefficient values (< 0.90), marked variations of the q_{cal} from that of q_{exp} and notable SSE values are found to be unfavorable for the system to obey pseudo-first order kinetic model.

Table 4.11 Pseudo-First- Order/ Pseudo- Second- Order Kinetics

Time (min)	Pb(II)			Cd(II)			Ni(II)		
	$\log (q_e-q_t)$	q_t	t/q_t	$\log (q_e-q_t)$	q_t	t/q_t	$\log (q_e-q_t)$	q_t	t/q_t
10	1.90	20.99	0.47	1.86	18.77	0.53	1.89	29.66	0.33
20	1.91	17.86	1.11	1.86	17.46	1.14	1.90	25.70	0.77
30	1.93	13.89	2.15	1.87	16.70	1.79	1.91	23.73	1.26
40	1.92	15.88	2.51	1.87	19.75	2.02	1.90	24.72	1.61
50	1.92	18.86	2.65	1.87	18.12	2.75	1.90	28.67	1.74
60	1.92	21.83	2.74	1.87	19.73	3.04	1.91	29.66	2.02

Table 4.12 Comparison of Pseudo-First-Order/ Pseudo-Second-Order Kinetic Constants

Conc. of Metal Ions (mg/L)	$q_{exp.}$ (mg/g)	Pseudo-First-Order Kinetics				Pseudo-Second-Order Kinetics			
		$q_{cal.}$ (mg/g)	$k_1\times10^{-3}$ (min^{-1})	R^2	SSE	$q_{cal.}$ (mg/g)	$k_2\times10^{-3}$ (g/ mg min)	R^2	SSE
Pb(II)									
50	9.91	16.66	1.38	0.8693	1.12	10.11	4.17	0.9855	0.03
100	14.22	22.64	2.78	**0.9119**	**0.26**	15.47	16.37	**0.9912**	**0.20**
150	11.82	21.30	1.19	0.8888	0.07	12.63	1.25	0.9910	0.30
200	12.65	21.63	2.02	0.8852	0.16	13.93	4.47	0.9975	0.37
250	13.86	18.51	1.52	0.7920	0.27	12.91	0.72	0.9902	0.80
Cd(II)									
50	8.06	13.23	0.06	0.9120	0.87	7.38	4.00	0.9861	1.22
100	13.68	22.35	1.95	**0.8810**	**0.33**	14.75	5.97	**0.9913**	**0.17**
150	11.64	23.92	1.58	0.8435	0.54	12.84	2.74	0.9832	1.03
200	12.72	24.45	1.86	0.8424	0.04	11.18	0.23	0.9815	0.58
250	12.98	29.08	2.37	0.8677	0.64	12.95	0.47	0.9914	0.00
Ni(II)									
50	7.38	14.71	0.01	0.8502	1.22	9.56	8.18	0.9832	0.36
100	12.52	21.33	0.27	**0.8773**	**0.13**	13.86	11.36	**0.9901**	**0.22**
150	10.15	17.00	0.23	0.8673	0.02	9.61	4.32	0.9892	0.25
200	10.97	14.82	0.66	0.8202	0.64	10.08	0.16	0.9765	0.64
250	11.49	16.41	0.89	0.8776	0.81	10.69	0.68	0.9904	0.13

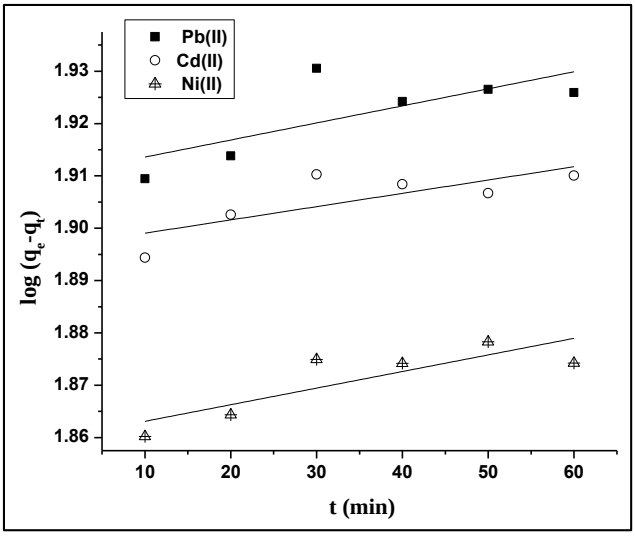

Figure 4.25 Pseudo-First-Order Kinetics

4.8.2 Pseudo-Second-Order Model

Figure 4.26 exhibits the pseudo second-order plot of t/q_t vs t, the slopes and intercepts of which were used to calculated q_{cal} and K_2 (Table 4.12). The higher q_{cal} value for the optimized concentrations of 100 mg/L, against other concentrations supports greater driving force of metal ions[100], thereby employing more efficient utilization of TPJB (higher concentration gradient pressure). A declining rate constant value (k_2) indicate a diminishing diffusion of metal ions[143] onto the TPJB surface. It is evident that, a relatively higher R^2 values and lower SSE values[144] of pseudo second order kinetic against pseudo first order kinetic model, support better fit of the former, applicable to Pb(II), Cd(II) and Ni(II) – TPJB systems.

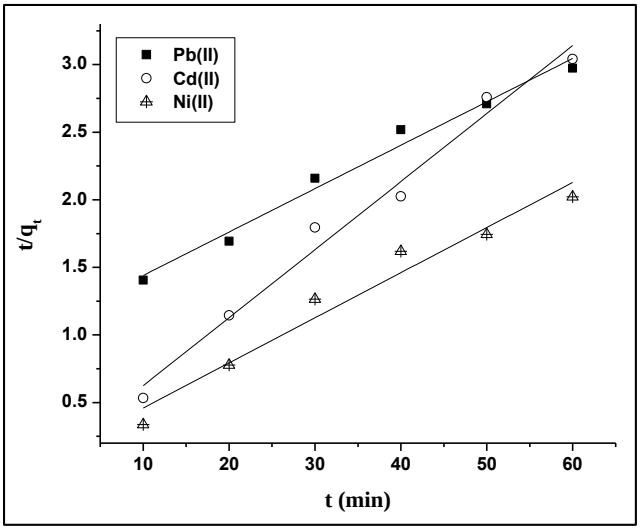

Figure 4.26 Pseudo-Second-Order Kinetics

4.8.3 Elovich Model

The kinetic constants α and β were derived from the intercepts and slopes of the Elovich plot, ln t vs q_t (Figure 4.27). It is obvious from the table 4.13, that the adsorption rate constant α and extent of surface coverage β are inversely related at increasing concentrations of Pb(II), Cd(II) and Ni(II) ions. This could be attributed to the fact that lesser active sites are available[145] in TPJB surface for higher concentrations, which reflects in the β values. Similar findings have been reported for the removal of Pb(II) onto acorn waste[127].

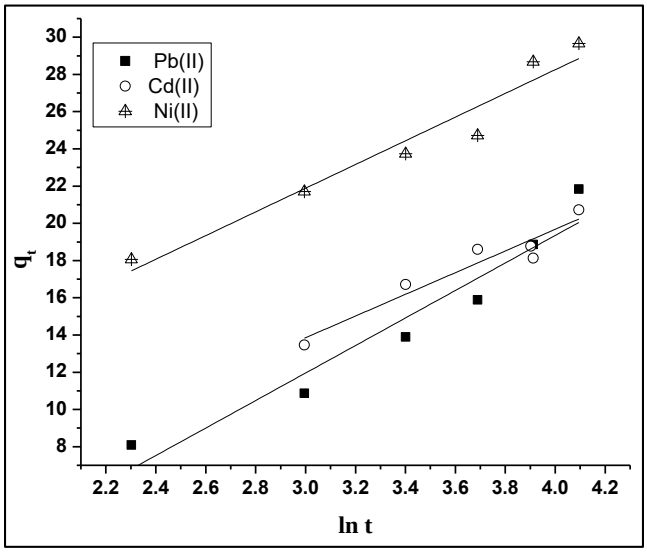

Figure 4.27 Elovich Model

Table 4.13 Elovich Constants

Conc. of Metal Ions (mg/L)	Pb(II)			Cd(II)			Ni(II)		
	α	β	R^2	α	β	R^2	α	β	R^2
50	1.88	15.16	0.9277	4.49	5.51	0.9287	2.93	7.75	0.9285
100	5.62	14.06	0.9243	3.93	4.21	0.9245	5.51	6.44	0.9634
150	5.44	14.09	0.9512	8.92	1.36	0.9218	6.30	5.86	0.9398
200	8.41	7.15	0.9364	10.19	3.93	0.9145	10.53	6.21	0.9377
250	11.37	5.09	0.9298	7.89	3.21	0.9293	9.91	5.29	0.9086

α: (mg/g min), β: (g/mg)

4.8.4 Intraparticle Diffusion Model

The plot of q_t vs $t_{1/2}$ (Figure 4.28) at varying initial concentrations, reveal two distinct portions [94, 146]. The first portion refers to the boundary layer diffusion and the second slightly distorted part corresponds to a gradual adsorption, the intraparticle diffusion being the rate limiting step. The intraparticle diffusion rate constant 'Ki' and boundary layer thickness 'C' (Table 4.14) are found to increase with initial concentrations due to the utilization of most readily available sites on the TPJB surface. The deviation in linear plot from origin can be attributed to the mass transfer resistance in the initial and final stages of the adsorption [147, 148, 149].

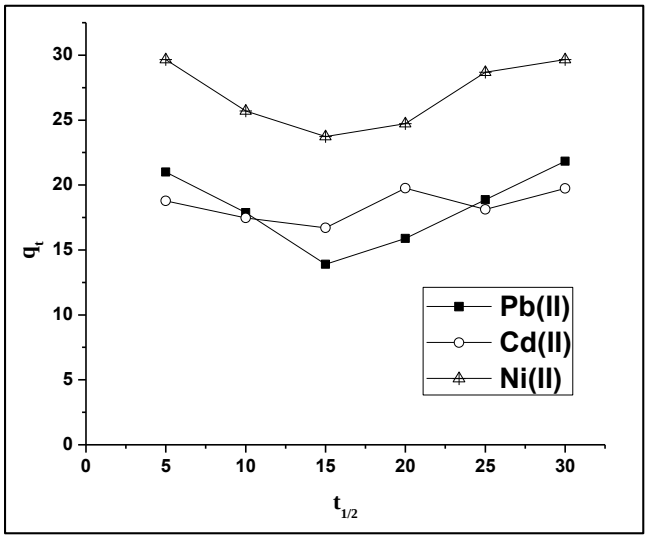

Figure 4.28 Intraparticle Diffusion Model

Table 4.14 Intraparticle Diffusion Constants

Conc. of Metal Ions (mg/L)	Pb(II)		Cd(II)		Ni(II)	
	K_i (mg/g $min^{1/2}$)	C	K_i (mg/g $min^{1/2}$)	C	K_i (mg/g $min^{1/2}$)	C
50	0.13	6.74	0.17	12.33	0.20	14.08
100	0.41	7.83	0.27	12.71	0.19	18.30
150	0.39	26.60	0.46	24.43	0.40	38.69
200	0.52	56.97	0.73	55.68	0.76	48.68
250	0.79	75.79	0.55	100.37	0.66	98.99

4.9 Adsorption Dynamics

From the Van't Hoff plot, (Figure 4.29) variations in enthalpy and entropy values are calculated (Table 4.15). The positive ΔH^0 and ΔS^0 values indicate presence of an energy barrier supporting endothermicity[150] and the increased randomness[140] between TPJB and studied metal ions respectively. Free energy variations (ΔG^0) describe the feasibility and spontaneity of the process[141, 108]. Similar observations had been recorded for the sorption studies using rice bran[151], tree fern[152] and rubber wood sawdust[153].

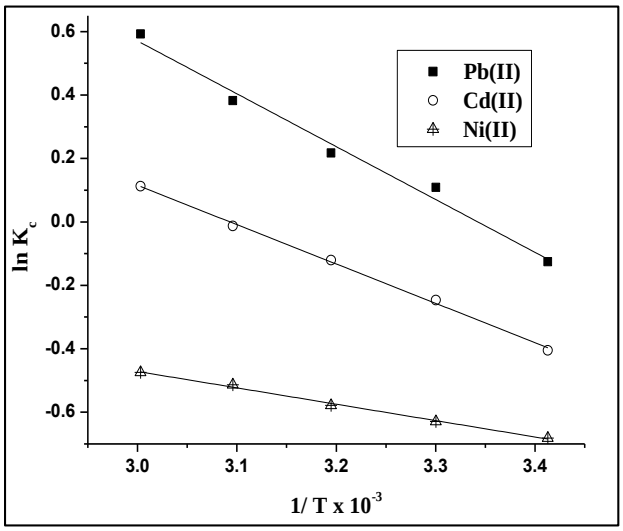

Figure 4.29 Vant Hoff's Plot

Table 4.15 Thermodynamic Constants

Temp. K	Pb(II)			Cd(II)			Ni(II)		
	ΔG°x10^{-3} kJ/ mol	ΔH° kJ/ mol	ΔS° J/ mol K	ΔG°x10^{-3} kJ/ mol	ΔH° kJ/ mol	ΔS° J/ mol K	ΔG°x10^{-3} kJ/mol	ΔH° kJ/ mol	ΔS° J/ mol K
293	-1.34	13.85	41.30	-1.96	10.30	21.88	-2.60	4.29	8.95
303	-6.01			-6.21			-1.58		
313	-6.81			-3.14			-1.50		
323	-8.91			-3.13			-1.37		
333	-1.63			-3.12			-1.31		

4.10 Effect of TPJB on Effluent/ Synthetic Solutions

Figure 4.30 depicts the sorption trend of TPJB at varying doses against study paint effluent [Pb(II)] and synthetic solutions [Cd(II) and Ni(II)]. A maximum of 79 %, 74 % and 71% removal of Pb(II), Cd(II) and Ni(II) from their respective samples after the appropriate dilutions (mentioned in 3.12) is evident at an optimized dose of 500 mg TPJB, in case of all the three divalent ions. This implies an appreciable metal removal efficiency of TPJB for the samples in presence of other interfering ions i.e., under native conditions.

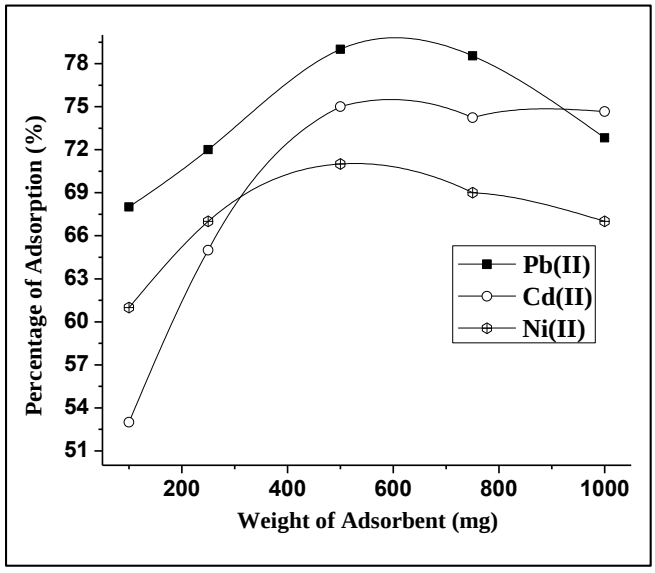

Figure 4.30 Effect of TPJB on Effluent/ Synthetic Solutions